JEM Journal of Experimental Medicine

TECHNICAL ADVANCES AND RESOURCES

Mapping and role of T cell response in SARS-CoV-2–infected mice

Zhen Zhuang[1*], Xiaomin Lai[1*], Jing Sun[1*], Zhao Chen[1*], Zhaoyong Zhang[1*], Jun Dai[2*], Donglan Liu[1*], Yuming Li[1*], Fang Li[1*], Yanqun Wang[1], Airu Zhu[1], Junxiang Wang[1], Wenhui Yang[3], Jicheng Huang[2], Xiaobo Li[2], Lingfei Hu[3], Liyan Wen[1], Jianfen Zhuo[1], Yanjun Zhang[1], Dingbin Chen[1], Suxiang Li[1], Shuxiang Huang[2], Yongxia Shi[2], Kui Zheng[2], Nanshan Zhong[1], Jingxian Zhao[1], Dongsheng Zhou[3], and Jincun Zhao[1,4]

Virus-specific T cells play essential roles in protection against multiple virus infections, including SARS-CoV and MERS-CoV. While SARS-CoV-2–specific T cells have been identified in COVID-19 patients, their role in the protection of SARS-CoV-2–infected mice is not established. Here, using mice sensitized for infection with SARS-CoV-2 by transduction with an adenovirus expressing the human receptor (Ad5-hACE2), we identified SARS-CoV-2–specific T cell epitopes recognized by CD4$^+$ and CD8$^+$ T cells in BALB/c and C57BL/6 mice. Virus-specific T cells were polyfunctional and were able to lyse target cells in vivo. Further, type I interferon pathway was proved to be critical for generating optimal antiviral T cell responses after SARS-CoV-2 infection. T cell vaccination alone partially protected SARS-CoV-2–infected mice from severe disease. In addition, the results demonstrated cross-reactive T cell responses between SARS-CoV and SARS-CoV-2, but not MERS-CoV, in mice. Understanding the role of the T cell response will guide immunopathogenesis studies of COVID-19 and vaccine design and validation.

Introduction

A new betacoronavirus, severe acute respiratory syndrome coronavirus 2 (SARS-CoV-2), emerged in Wuhan, China, in December 2019 as the etiological agent of coronavirus disease 2019 (COVID-19; Zhou et al., 2020), prompting the World Health Organization in January 2020 to declare an international public health emergency. As of December 5, 2020, it has infected >65 million people worldwide with >1 million deaths.

Virus clearance during primary respiratory virus infections depends on the generation of an effective virus-specific CD4$^+$ and CD8$^+$ T cell response (Christensen et al., 2000; Zhao et al., 2010; Zhong et al., 2001). While respiratory virus infections sometimes elicit transient antibody responses, virus-specific T cells are often more durable. For example, SARS-CoV–specific T cells could be detected as long as 17 yr after infection in SARS survivors (Le Bert et al., 2020). MERS-CoV–specific T cell responses were detected in most of the patients, including asymptomatic patients with undetectable antibody responses (Zhao et al., 2017). Recently, SARS-CoV-2–specific T cells were reported in acute phase and convalescent COVID-19 patients, and these T cells were closely related to disease severity (Grifoni et al., 2020; Peng et al., 2020; Sekine et al., 2020; Weiskopf et al., 2020).

In addition, cross-reactive T cells had been found in SARS-CoV-2–unexposed individuals, indicating preexisting cross-reactive T cells against seasonal respiratory CoVs or as-yet unidentified pathogens might play a role in COVID-19 immunopathogenesis (Braun et al., 2020; Le Bert et al., 2020; Mateus et al., 2020).

Mice are the ideal animals for pathogenesis studies and the evaluation of new therapies and vaccines. Our previous studies identified SARS-CoV– and MERS-CoV–specific CD4$^+$ and CD8$^+$ T cells in mice, determined by IFN-γ expression after epitope peptide stimulation (Zhao et al., 2007; Zhao et al., 2014; Zhao et al., 2010). CD4$^+$ and CD8$^+$ T cell–deficient SCID and RAG$^{-/-}$ mice had delayed viral clearance (Zhao et al., 2010). Reduced SARS-CoV–specific CD8$^+$ T cell responses in the lungs of aged mice were associated with increased mortality rate (Zhao et al., 2011). MERS-CoV–specific CD8$^+$ T cells were also required for

[1]State Key Laboratory of Respiratory Disease, National Clinical Research Center for Respiratory Disease, Guangzhou Institute of Respiratory Health, First Affiliated Hospital of Guangzhou Medical University, Guangzhou, China; [2]Guangzhou Customs District Technology Center, Guangzhou, China; [3]State Key Laboratory of Pathogen and Biosecurity, Beijing Institute of Microbiology and Epidemiology, Beijing, China; [4]Institute of Infectious Disease, Guangzhou Eighth People's Hospital of Guangzhou Medical University, Guangzhou, China.

*Z. Zhuang, X. Lai, J. Sun, Z. Chen, Z. Zhang, J. Dai, D. Liu, Y. Li, and F. Li contributed equally to this paper; Correspondence to Jincun Zhao: zhaojincun@gird.cn; Dongsheng Zhou: dongshengzhou1977@gmail.com; Jingxian Zhao: zhaojingxian@gird.cn.

viral clearance in infected C57BL/6 and BALB/c mice (Zhao et al., 2014). Together these results support a critical role of T cells for virus clearance in CoV-infected mice.

Recently, we generated a mouse model for COVID-19 by exogenous delivery of human ACE2 (hACE2) with a replication-deficient adenovirus (Ad5-hACE2; Sun et al., 2020). Ad5 transduction could support CoV replication in mouse lung as long as 17–22 d after transduction (Zhao et al., 2014). Ad5-hACE2–sensitized mice developed pneumonia characterized by weight loss, severe pulmonary pathology, and high-titer virus replication in lungs as well as robust anti-virus adaptive immune responses. Ad5-hACE2–transduced mice enable studies of immunopathogenesis and rapid assessments of antiviral and vaccine candidates. Thus far, no $CD4^+$ or $CD8^+$ T cell epitopes have been identified in SARS-CoV-2–infected mice, and the functional characterization of virus-specific T cells is incomplete.

Here, using the Ad5-ACE2–transduced mice, we identified SARS-CoV-2–specific T cell epitopes in BALB/c and C57BL/6 mice. We show that SARS-CoV-2–specific $CD4^+$ T and $CD8^+$ T cells were polyfunctional and cytolytic and that T cell vaccination in the absence of neutralizing antibodies protected mice from SARS-CoV-2 infection. In addition, cross-reactive T cell responses were found between SARS-CoV and SARS-CoV-2 but not MERS-CoV in mice. This study sheds light on immunopathogenesis studies and vaccine design and validation in vivo.

Results

Identification of $CD4^+$ and $CD8^+$ T cell epitopes in SARS-CoV-2–infected WT BALB/c and C57BL/6 mice

To map MHC class I–restricted $CD8^+$ and MHC class II–restricted $CD4^+$ T cell epitopes, a set of 20-mer peptides overlapping by 10 amino acids were synthesized covering the four SARS-CoV-2 structural proteins (the spike [S] glycoprotein, the nucleocapsid [N] protein, and the transmembrane [M] and envelope [E] proteins), and the six putative accessory proteins (ORF3a, ORF6, ORF7a, ORF8, ORF9b, and ORF9c). Initially, Venezuelan equine encephalitis replicon particles (VRPs) expressing SARS-CoV-2-S, SARS-CoV-2 N, SARS-CoV-2 M, SARS-CoV-2 E, ORF3a, ORF6, ORF7a, ORF8, ORF9b, and ORF9c were generated. Mice were vaccinated with each VRP i.n., and 7 d after vaccination, cells were isolated from lungs and stimulated with 5 μM of each 20-mer peptide or 10-μM peptide pool of each protein for 5–6 h in the presence of brefeldin A in 96-well U-bottom plates. Antigen-specific T cells were identified by IFN-γ production using intracellular cytokine staining (ICS). For BALB/c ($H\text{-}2^d$–restricted) mice, six peptides (N-7, N-25, N-36, S-7, S-45, and ORF8-5; Fig. S1 A), and four peptides (N-9, S-27, S-54, and S-106; Fig. S1 B) were able to stimulate $CD4^+$ and $CD8^+$ T cells, respectively, to produce IFN-γ as compared with no peptide controls. For C57BL/6 ($H\text{-}2^b$–restricted) mice, seven peptides (N-1, S-3, S-7, ORF3a-16, ORF3a-27, ORF3a-28, and ORF7a-7; Fig. S2 A), and 24 peptides (M-18, N-11, N-22, N-23, N-28, S-8, S-10, S-13, S-14, S-22, S-23, S-24, S-26, S-27, S-48, S-51, S-52, S-54, S-55, S-57, S-82, ORF3a-11, ORF7a-9, and ORF7a-10; Fig. S2 B) were able to stimulate $CD4^+$ and $CD8^+$ T cells, respectively, from VRP-vaccinated mice. Of note, VRP vaccination could induce a high level of foreign gene expression and efficiently induce humoral and T cell responses in mice, as we described previously (Sun et al., 2020; Zhao et al., 2016). It is unlikely to miss dominant T cell epitopes using our mapping methods; however, we cannot rule out the possibility. These peptides were further analyzed using T cell epitope consensus servers (Rankpep, Immune Epitope Database and Analysis Resource, and SYFPEITHI; Dhanda et al., 2019; Rammensee, 1995; Reche et al., 2004). Serially truncated peptides were synthesized and were used to identify precise epitopes using cells derived from lungs of vaccinated BALB/c and C57BL/6 mice. As shown in Fig. S1 (C and D) and Fig. S2 (C and D), the truncated peptides that induced the most robust T cell responses in the set of truncated peptides from the same one 20-mer peptide were selected as candidate T cell epitope peptides.

To confirm these epitopes, BALB/c and C57BL/6 mice were transduced with Ad5-ACE2 and after 5 d were infected i.n. with 1×10^5 PFU of SARS-CoV-2 (Sun et al., 2020). Bronchoalveolar lavage fluids (BALFs) were harvested 8 d post-infection (d.p.i.). Cells were then stimulated with all the indicated candidate epitope peptides, respectively. T cell responses were determined by IFN-γ production using ICS. A total of 6 $I\text{-}A^d$–restricted $CD4^+$ T cell epitopes (Fig. 1 A), 3 $H\text{-}2K/D/L^d$–restricted $CD8^+$ T cell epitopes (Fig. 1 B; BALB/c mice), 5 $I\text{-}A^b$–restricted $CD4^+$ T cells (Fig. 1 C), and 10 $H\text{-}2K/D^b$–restricted $CD8^+$ T cell epitopes (Fig. 1 D; C57BL/6 mice) were confirmed. Of note, several epitope candidates that were identified in VRP-vaccinated mice were not presented in SARS-CoV-2–infected mice, which may reflect the differences in viral protein expression levels in infected mice (Kim et al., 2020) or direct competition between epitopes in vivo. Epitopes and their MHC restrictions are summarized in Table 1. Dominant $CD4^+$ T cell epitopes, N351-365 (N351) in BALB/c mice and ORF3a 266–280 (ORF3a 266) in C57BL/6 mice, and dominant $CD8^+$ T cell epitopes, S535-543 (S535) in BALB/c mice and S538-546 (S538) in C57BL/6 mice, were selected for further study.

Kinetics of virus-specific T cell responses in SARS-CoV-2–infected BALB/c and C57BL/6 mice

To understand the dynamics of SARS-CoV-2–specific T cell responses after SARS-CoV-2 infection, infected WT BALB/c and C57BL/6 mice were euthanized at 5, 8, and 10 d.p.i. Cells were harvested from BALF, lung tissues, lung draining LNs (DLNs), and spleens and stimulated with indicated dominant $CD4^+$ or $CD8^+$ T cell epitope peptides. The frequency of IFN-γ^+ $CD4^+$ T cells recognizing N351 peptide peaked at 8–10 d.p.i., and maximum cell numbers were observed at 8 d.p.i. in airway (Fig. 2 A), lung tissues (Fig. 2 B), DLNs (Fig. S3 A), and spleens (Fig. S3 B) of BALB/c mice. SARS-CoV-2–S535–specific $CD8^+$ T cell responses also peaked at day 8 after infection in BALB/c mice and underwent quickly contraction from 8 d.p.i. (Fig. 2, C and D; Fig. S3 C; and Fig. S4 D). The kinetics of SARS-CoV-2–specific $CD4^+$ and $CD8^+$ T cell responses targeting ORF3a 266 (Fig. 2, E and F; and Fig. S3, E and F) and S538 (Fig. 2, G and I; and Fig. S3, G and I) peptides,

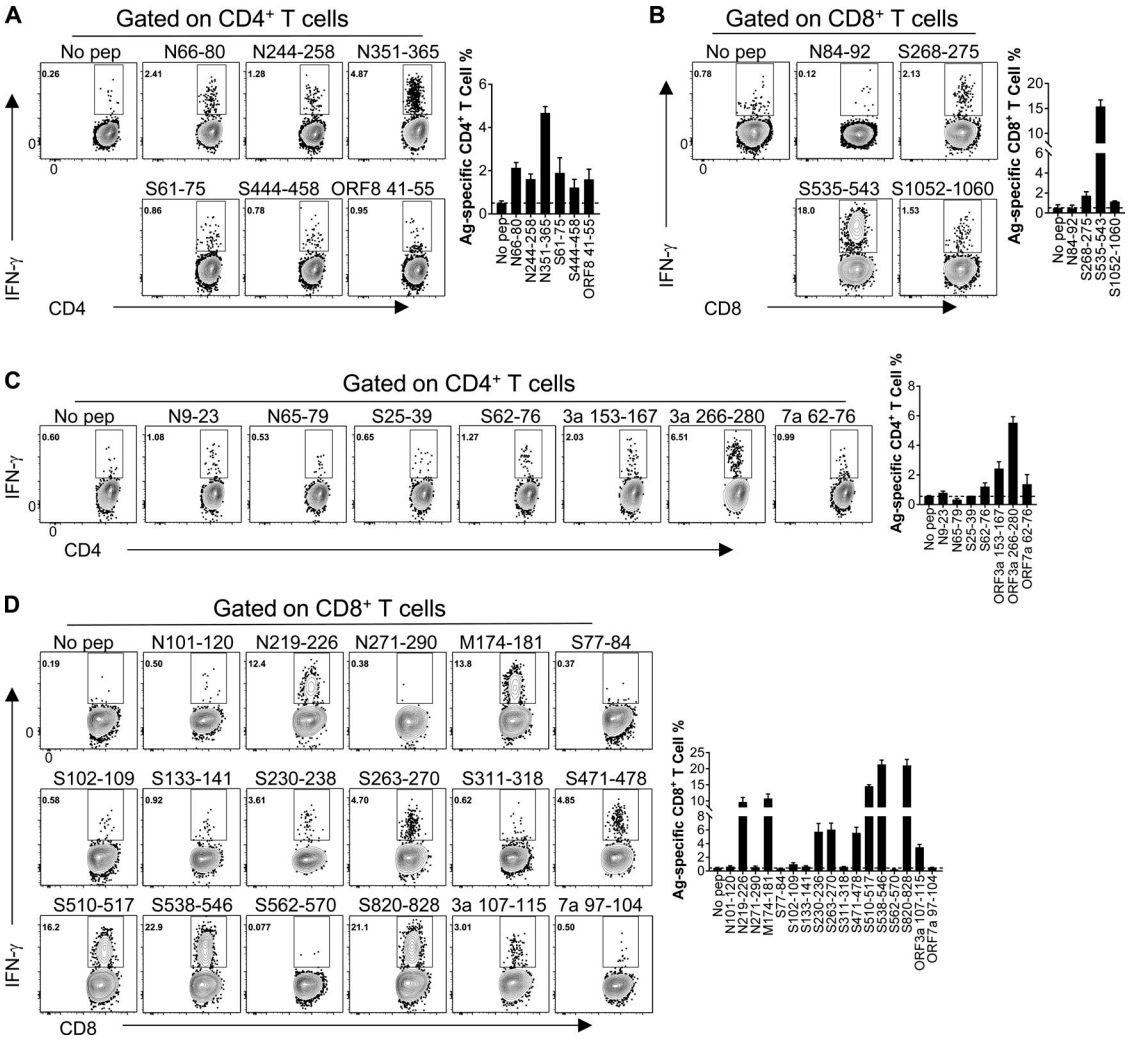

Figure 1. **Identification of CD4⁺ and CD8⁺ T cell epitopes in SARS-CoV-2–infected WT BALB/c and C57BL/6 mice. (A and B)** Confirmation of CD4⁺ T cell epitopes (A) and CD8⁺ T cell epitopes (B) in infected BALB/c mice. Flow plots and summary columns are shown (n = 3; data verified in two independent experiments). **(C and D)** Confirmation of CD4⁺ T cell epitopes (C) and CD8⁺ T cell epitopes (D) in infected C57BL/6 mice. Flow plots and summary columns are shown (n = 3; data verified in two independent experiments). All results are expressed as mean ± SEM. Ag, antigen; pep, peptide.

respectively, shared similar trends to those observed in BALB/c mice in airway, lung tissues, DLNs, and spleens of transduced/infected C57BL/6 mice. The frequencies of SARS-CoV-2–specific T cells in the airway were much higher than T cells in the lungs, DLNs, and spleens. Virus-specific T cells in the airway, which first encounter viral antigen, were critical for mediating protection after SARS-CoV and MERS-CoV challenge (Zhao et al., 2016).

SARS-CoV-2–specific CD4⁺ T cells and CD8⁺ T cells were polyfunctional

Next, we aimed to characterize the phenotypes and functions of SARS-CoV-2–specific T cell responses, especially cells in the airway of infected mice. N351-CD4⁺ T cells and S535-CD8⁺ T cells from airway of transduced/infected BALB/c mice were identified by IFN-γ expression at 8 d.p.i. Phenotypes of virus-specific cells were determined by flow cytometry. Activation markers (CD44, CD43, CD11a, CD49d, CD27, and CD69) were up-regulated as expected after antigen encounter on both N351-CD4⁺ T cells (Fig. 3 A) and S535-CD8⁺ T cells (Fig. 3 E). Adhesion molecules (CD11a and CD49d; McDermott and Varga, 2011; Rai et al., 2009) and chemokine receptors (CXCR3, CXCR6, and CCR5) were also up-regulated, which possibly assisted T cell migration and localization to the airway (Fig. 3, A and E). The expression levels of L-selectin (CD62L) and the chemokine receptor (CCR7), which guide T cells to LNs, were reduced (Fig. 3, A and E). CD103 and Ly6C were expressed on S535-CD8⁺ T cells but not N351-CD4⁺ T cells, which was consistent with previous studies (Fig. 3, A and E; Brummelman et al., 2018; Yamanouchi et al., 1998). Functional markers (CD107a/b) related to T cell cytotoxicity were expressed on both N351-CD4⁺ T cells and S535-CD8⁺ T cells (Peters et al., 1991), which was consistent with the observation that N351-specific CD4⁺ T cells and S535-specific CD8⁺ T cells were able to lyse peptide pulsed target cells in vivo (Fig. 3, D and H). In addition to CD107a/b, CD40L was believed to be correlated with CD4⁺ T cell–mediated killing, which was not expressed on the

Table 1. **Characteristics of SARS-CoV-2–specific T cell epitopes in BALB/c mice and C57BL/6 mice**

Name	Sequence	Protein	Start position	End position	Length	MHC restriction
BALB/c						
N66-80	FPRGQGVPINTNSSP	N protein	66	80	15	I-A^d
N244-258	QTVTKKSAAEASKK	N protein	244	258	15	I-A^d
N351-365	ILLNKHIDAYKTFPP	N protein	351	365	15	I-A^d
S61-75	NVTWFHAIHVSGTNG	S protein	61	75	15	I-E^d
S444-458	KVGGNYNYLYRLFRK	S protein	444	458	15	I-A^d
ORF8 41-55	FYSKWYIRVGARKSA	ORF8	41	55	15	I-A^d
S268-275	GYLQPRTF	S protein	268	275	8	H2-K^d
S535-543	KNKCVNFNF	S protein	535	543	9	H2-D^d
S1052-1060	FPQSAPHGV	S protein	1052	1060	9	H-2L^d
C57BL/6						
N9-23	QRNAPRITFGGPSDS	N protein	9	23	15	I-A^b
S62-76	VTWFHAIHVSGTNGT	S protein	62	76	15	I-A^b
ORF3a 153-167	CYDYCIPYNSVTSSI	ORF3a	153	167	15	I-A^b
ORF3a 266-280	EPIYDEPTTTTSVPL	ORF3a	266	280	15	I-A^b
ORF7a 62-76	QFAFACPDGVKHVYQ	ORF7a	62	76	15	I-A^b
N219-227	LALLLLDRL	N protein	219	227	9	H2-D^b
M174-181	RTLSYYKL	M protein	174	181	8	H2-K^b
S102-109	RGWIFGTT	S protein	102	109	8	H2-K^b
S230-238	PIGINITRF	S protein	230	238	9	H2-D^b
S263-270	AAYYVGYL	S protein	263	270	8	H2-K^b
S471-478	EIYQAGST	S protein	471	478	8	H2-K^b
S510-517	VVVLSFEL	S protein	510	517	8	H2-K^b
S538-546	CVNFNFNGL	S protein	538	546	9	H2-D^b
S820-828	DLLFNKVTL	S protein	820	828	9	H2-D^b
ORF3a 107-115	YLYALVYFL	ORF3a	107	115	9	H2-D^b

virus-specific CD8$^+$ T cells (Coler et al., 2015; Fig. 3, A and E). Our finding showing CD4$^+$ T cells were cytotoxic was also consistent with previous reports (Brien et al., 2008; Zhou et al., 2018). Inhibitory molecules (CTLA-4 and PD-1) were up-regulated, while low levels of KLRG1 and high expression of CD127 were observed on N351-CD4$^+$ T cells, but higher on S535-CD8$^+$ T cells (Fig. 3, A and E). Phenotypic marker expression on S538-CD8$^+$ T cells of C57BL/6 mice was similar to S535-CD8$^+$ T cells in BALB/c mice (Fig. S4 A).

Airway N351-specific CD4$^+$ T cells and S535-specific CD8$^+$ T cells had superior effector function, indicated by the ability to produce more than three cytokines (IFN-γ, TNF, IL-10, and IL-2) at the same time (Fig. 3, B and F). S538-specific CD8$^+$ T cells in C57BL/6 mice primarily coproduced IFN-γ and TNF (Fig. S4 B). IL-10–producing virus-specific T cells were also found in SARS-CoV-2–infected mice, consistent with influenza A virus studies (Sun et al., 2009). Further, both virus-specific CD4$^+$ T cells and CD8$^+$ T cells in the airway exhibited greater function avidities than those in the lungs, indicating specific T cells in the airway were more sensitive to viral antigen simulation (Fig. 3, C and G; and Fig. S4 C).

Type I IFN (IFN-I) signaling was critical for the generation of robust T cell responses against SARS-CoV-2 infection

IFN-I is an important component of innate immunity, triggering an "antiviral state" in infected tissue (McNab et al., 2015; Perry et al., 2005). IFN-I also shapes the antiviral adaptive immune responses, including virus-specific T cell responses (González-Navajas et al., 2012; McNab et al., 2015). Immunocompromised COIVD-19 patients tend to have more severe disease and poor prognosis (Di Cosimo et al., 2020; Robilotti et al., 2020). To decipher the role of IFN-I in T cell responses after SARS-CoV-2 infection, kinetics and cytokine production of N351-CD4$^+$ T cells and S535-CD8$^+$ T cells in IFNAR (type I IFN receptor) KO BALB/c mice was investigated. Both virus-specific CD4$^+$ and CD8$^+$ T cell responses peaked at day 8 after infection (Fig. 4, A and B), as in WT BALB/c mice. However, both frequencies and cell numbers of N351-specific CD4$^+$ T cells and S535-specific CD8$^+$ T cells in IFNAR KO BALB/c mice were significantly lower than those in WT mice (Fig. 4, C and D). Further, although some of the IFNAR KO T cells were multifunctional as determined by expressing two cytokines (IFN-γ combined with TNF or IL-10 or IL-2), the frequency of bifunctional and

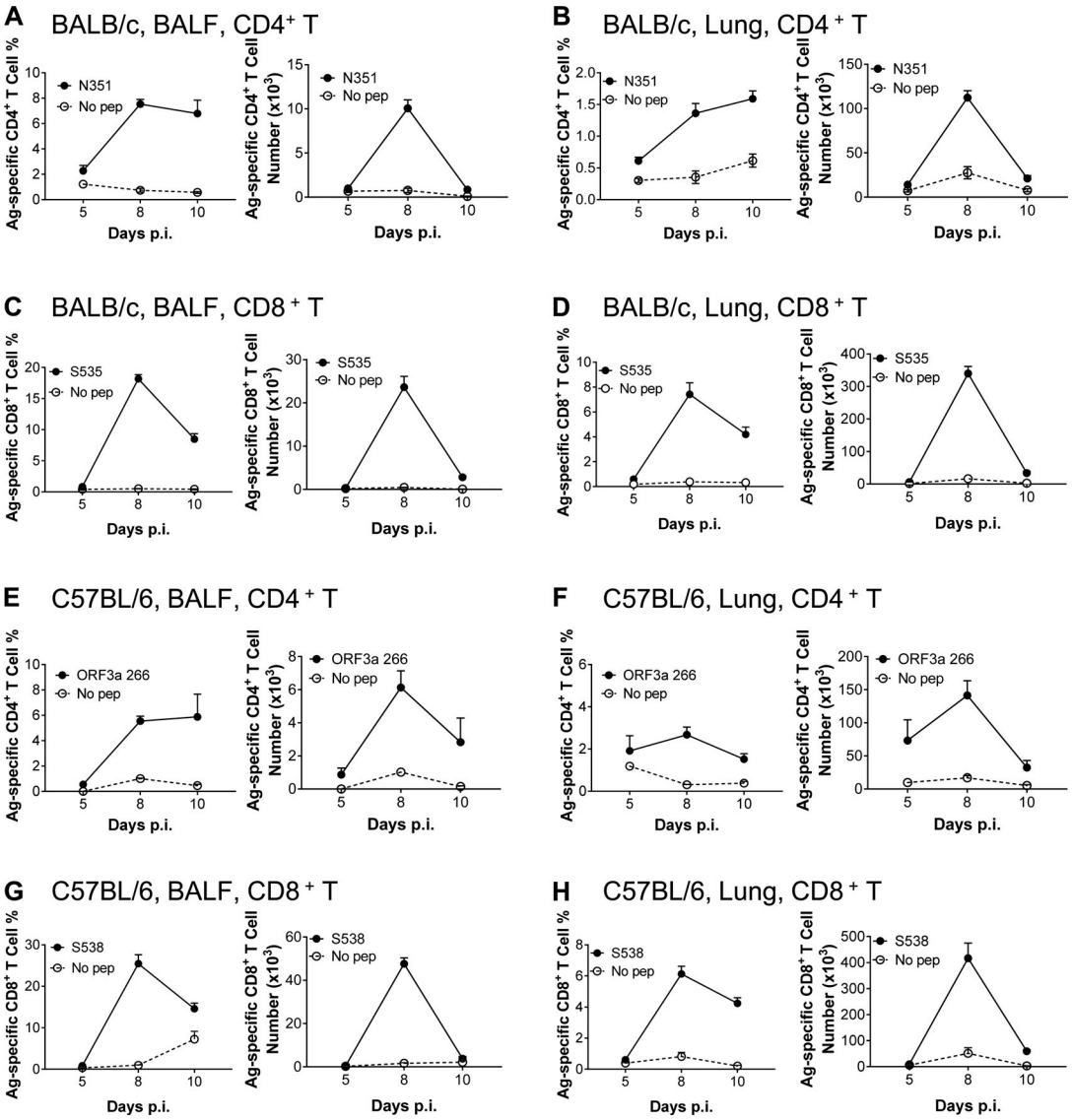

Figure 2. **Kinetics of virus-specific T cell responses in BALF and lung of SARS-CoV-2–infected BALB/c and C57BL/6 mice. (A–D)** Lymphocytes from airway and lung of transduced/infected WT BALB/c mice were harvested at indicated time points after infection and stimulated with 5 µM N351 (A and B) and 1 µM S535 (C and D) for 6 h in the presence of brefeldin A. The frequencies (left) and cell numbers of antigen-specific T cells (right) in BALF (A and C) and lung (B and D) are shown (n = 3 or 4 mice; data are representative of three independent experiments). **(E–H)** Lymphocytes from airway and lung of transduced/infected C57BL/6 mice were harvested at indicated time points and stimulated with 5 µM ORF3a 266 (E and F) and 1 µM S538 (G and H) for 6 h in the presence of brefeldin A. The frequencies (left) and cell numbers (right) of antigen-specific T cells are shown (n = 3 or 4 mice; data are representative of three independent experiments). All results are expressed as mean ± SEM. Ag, antigen; pep, peptide; p.i., post-infection.

polyfunctional cells was lower than in WT mice (Fig. 4, E and F). In addition, both virus-specific CD4+ T cells and CD8+ T cells in IFNAR KO mice exhibited lower functional avidity than those in WT mice (Fig. 4, G and H), indicating that loss of IFN-I signal reduced the sensitivity of virus-specific T cell to antigens, which possibly could be due to altered inflammation milieu in different strains of mice or higher viral antigen expression level in IFNAR KO mice. IFNAR KO mice had delayed weight gain and reduced kinetics of viral clearance at later phase of infection (days 4–6; Fig. 4 I), which could possibly be associated with compromised T cell responses since T cell responses started to emerge in the lung at this time after infection. These results indicated that IFN-I signaling was required for optimal SARS-CoV-2–specific T cell development and functionality.

Epitope-specific CD4+ and CD8+ T cells partially protected SARS-CoV-2–infected mice from severe disease

Next, we assessed whether SARS-CoV-2–specific T cells alone could protect mice from infection. A set of VRP vectors expressing only single immunodominant T cell epitopes was generated as described previously (Pushko et al., 1997; Zhao et al., 2016), including VRP-N351 (I-A^d, BALB/c), VRP-S535 (H-2D^d, BALB/c), and VRP-S358 (H-2D^b, C57BL/6). VRP-GFP was used as a control. Mice were vaccinated twice i.n. at 4-wk intervals and infected at day 28 after booster (Fig. 5 A). BALFs were harvested

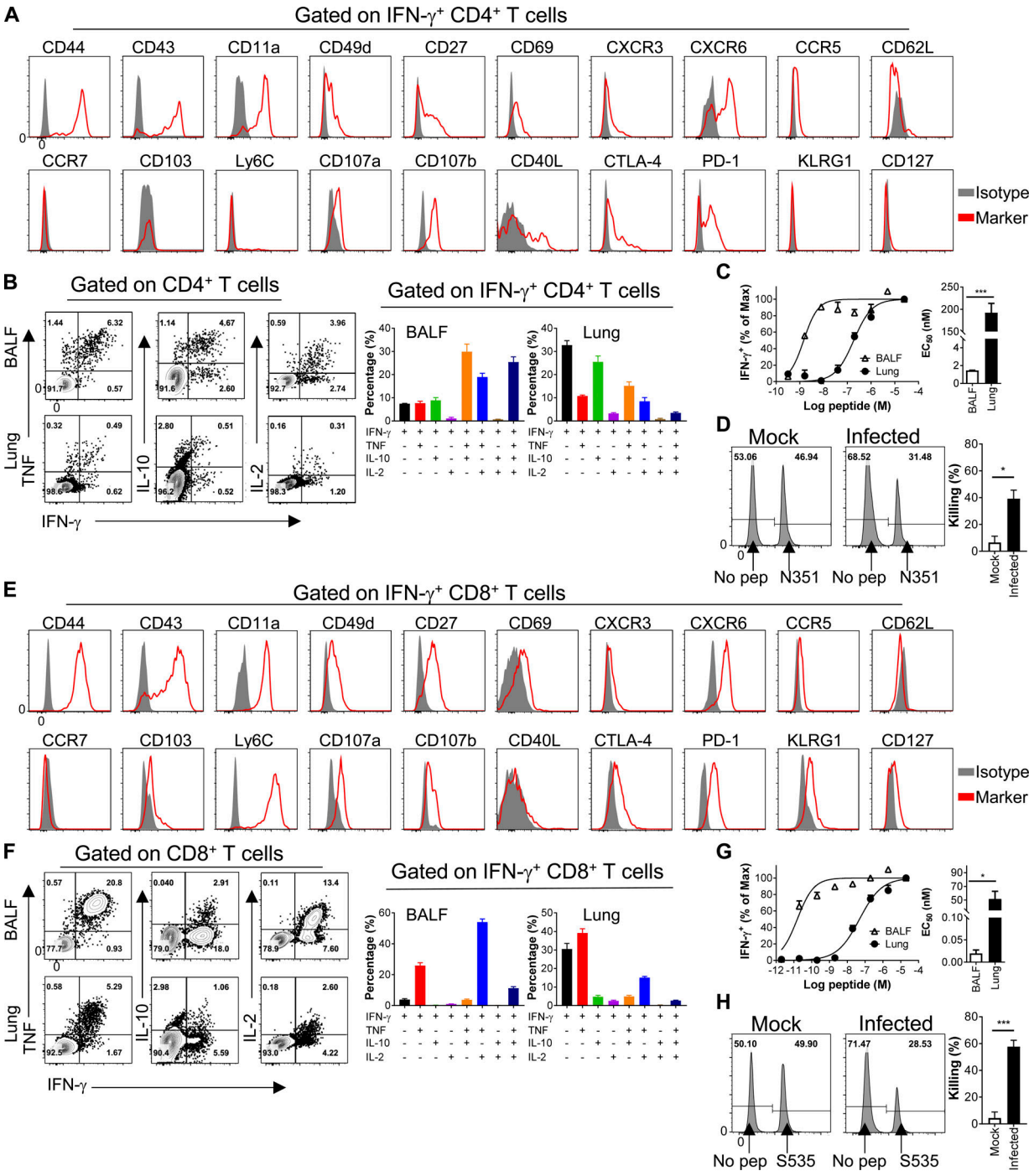

Figure 3. **SARS-CoV-2–specific CD4⁺ T cells and CD8⁺ T cells were polyfunctional. (A and E)** Phenotyping BALF-derived SARS-CoV-2-N351–specific CD4⁺ T cells (A) and SARS-CoV-2-S535–specific CD8⁺ T cells (E). **(B and F)** Cytokine expression of airway-derived N351-specific CD4⁺ T cells (B) and S535-specific CD8⁺ T cells (F) are shown (n = 3 mice; data are representative of two independent experiments). **(C and G)** Functional avidity curves (left) of airway- and lung-derived N351-specific CD4⁺ T cells (C) and S535-specific CD8⁺ T cells (G) and the amount of peptide required for half-maximum response (EC_{50}) are shown (right; n = 3 mice; data are representative of two independent experiments; Student's t tests; P value of C is 0.0004; P value of G is 0.0051). **(D and H)** Representative flow histograms (left) and killing rates (right) of in vivo cytotoxicity of N351-specific CD4⁺ T cells (D) and S535-specific CD8⁺ T cells (H) in SARS-CoV-2–infected mice and mock-infected mice are shown (n = 5 mice per group; data are representative of two independent experiments; Student's t tests; P value of D is 0.0062; P value of H is 0.0002). *, P < 0.05; ***, P < 0.0005. All results are expressed as mean ± SEM. Max, maximum; pep, peptide.

at the indicated time points (Fig. 5 A). Epitope-specific T cells were detected by intracellular IFN-γ staining. Vaccination with VRP-N351, S353, and S358 but not VRP-GFP induced epitope-specific T cell responses in the airways, which were increased by boosting and were recalled robustly after infection. Moderately decreased SARS-CoV-2 titers and reduced lung tissue pathological changes in mouse lungs were observed after immunization (Fig. 5, B–D). Neutralizing antibodies from different

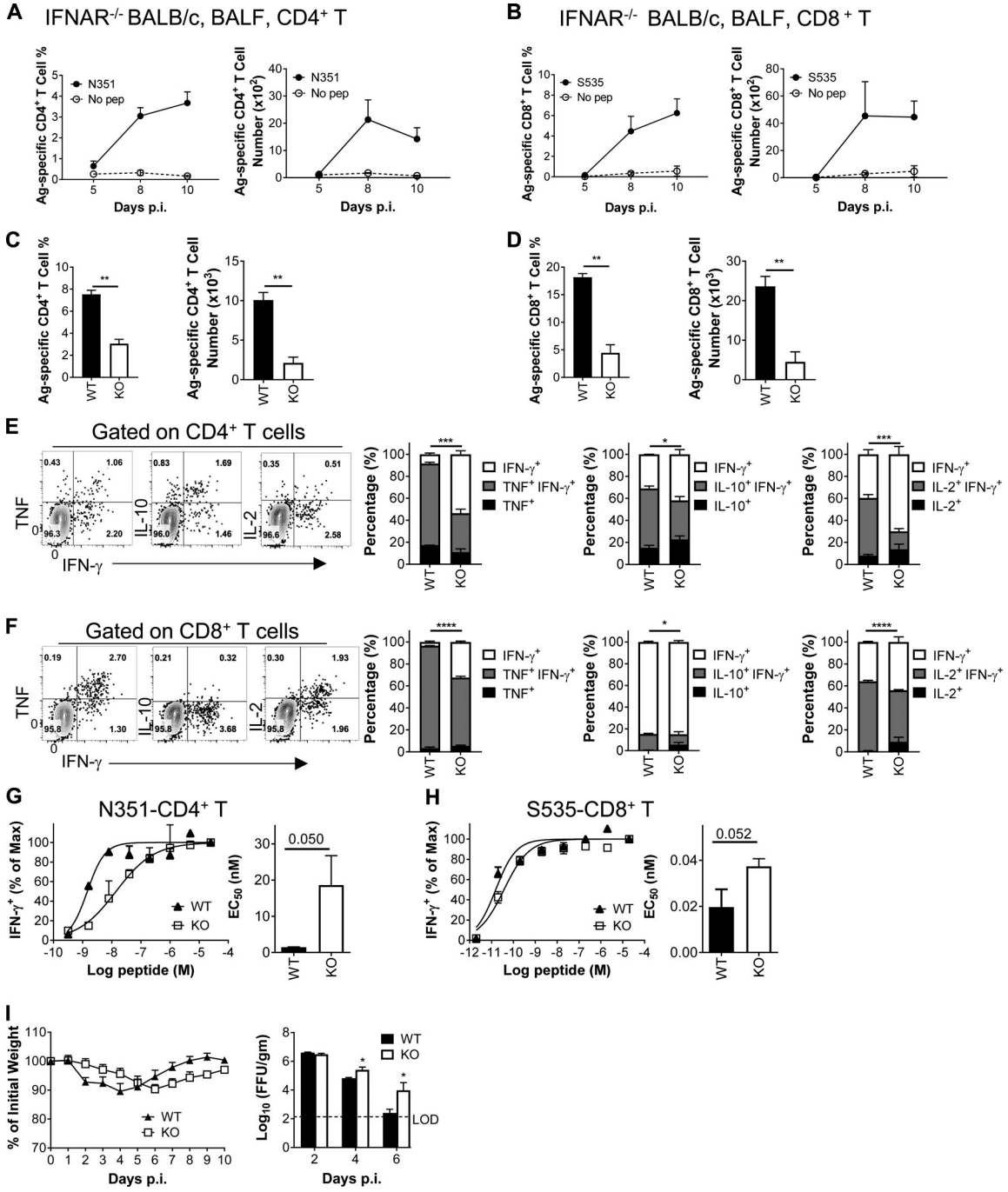

Figure 4. **IFN-I signaling was critical for the generation of robust T cell responses against SARS-CoV-2 infection. (A and B)** Frequencies (left) and cell numbers (right) of airway-derived N351-specific CD4+ T cells (A) and S535-specific CD8+ T cells (B) at indicated time points are shown (n = 3 or 4 mice per time point; data are representative of three independent experiments). **(C and D)** Airway-derived N351-specific CD4+ T cell responses (C) and S535-specific CD8+ T cell responses (D) in WT and KO BALB/c mice are compared (n = 3 or 4 mice; data are representative of two independent experiments; Student's t tests; P values of C are 0.0006 and 0.0013; P values of D are 0.0005 and 0.0029). **(E and F)** Representative flow plots of N351-specific CD4+ T cells (E) and S535-specific CD8+ T cells (F) are shown (left). Bi-cytokine expression capability (right three panels) is statistically different between WT and KO mice (n = 3 or 4 mice; data are representative of two independent experiments; Student's t tests; P values of E are 0.0003, 0.0057, and 0.0004; P values of F are <0.0001, 0.0445, and <0.0001). **(G and H)** Functional avidity curves (left) of N351-specific CD4+ T cells (G) and S535-specific CD8+ T cells (H) in KO and WT mice and the amount of peptide required for half-maximum response (EC_{50}) are shown (right; n = 3 mice; data are representative of two independent experiments; Student's t tests; P value of G is 0.050; P value of H is 0.052). **(I)** Weight loss and viral titers in the lungs were measured at the indicated time points (n = 3–5 mice per group per time point for viral titer; data are representative of two independent experiments; Student's t tests; P values are 0.0291 and 0.0394). *, P < 0.05; **, P < 0.005; ***, P < 0.0005; ****, P < 0.0001. All results are expressed as mean ± SEM. Ag, antigen; FFU, focus-forming unit; Max, maximum; pep, peptide; p.i., post-infection.

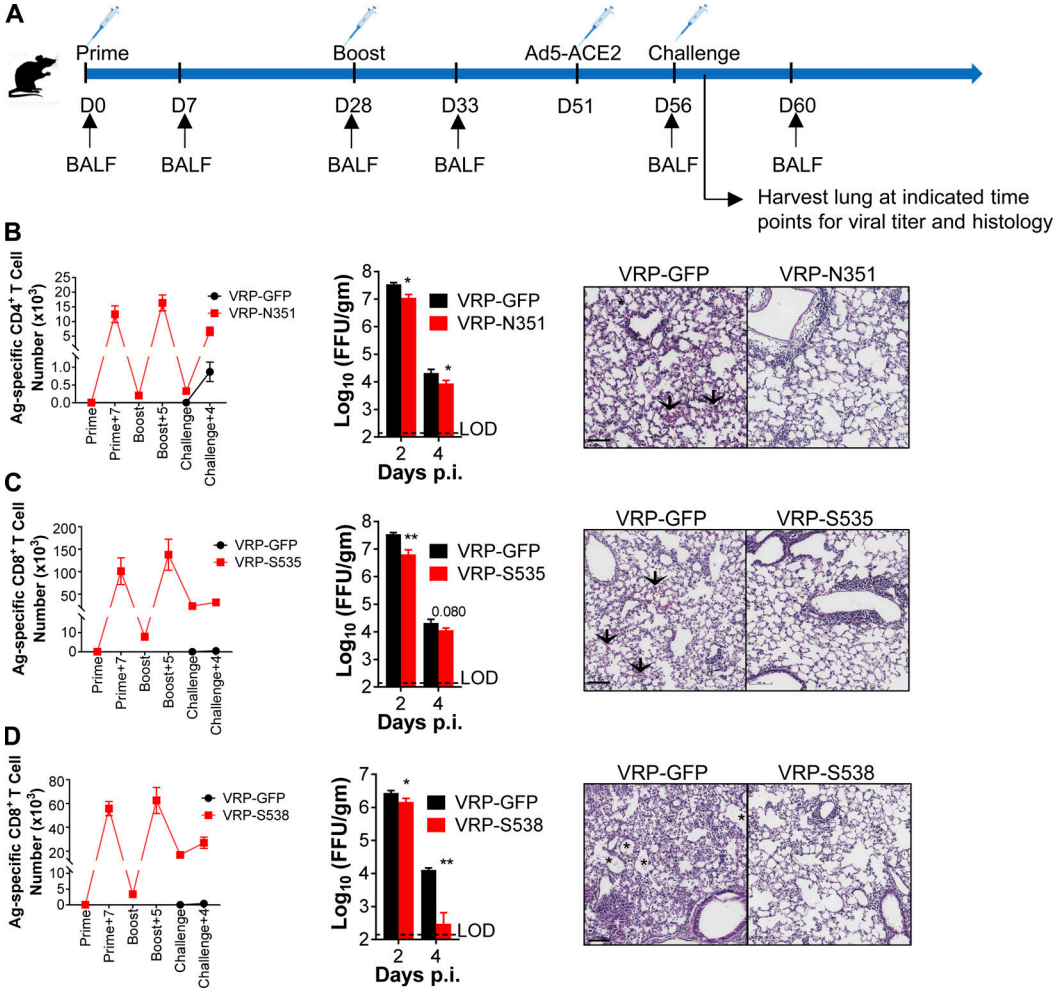

Figure 5. **Epitope-specific CD4⁺ and CD8⁺ T cells partially protected SARS-CoV-2–infected mice from severe disease. (A)** Strategy of VRP vaccination and SARS-CoV-2 challenge. **(B and C)** Effects of N351-specific CD4⁺ T cells (B) and S535-specific CD8⁺ T cells (C) in BALB/c mice. Cell numbers of airway-derived antigen-specific T cells are shown (n = 3 or 4 mice per group per time point; left). Viral titers in the lungs were measured at the indicated time points (n = 4 mice per group per time point; middle; data are representative of at least two independent experiments; Student's t tests; P values of B are 0.0051 and 0.0403; P values of C are 0.0026 and 0.0804). Sections of paraffin-embedded lungs from infected mice at 4 d.p.i. were stained with hematoxylin/eosin (n = 3 mice per group per time point; right; data are representative of at least two independent experiments). Scale bar, 100 mm. **(D)** Effects of S538-specific CD8⁺ T cells in C57BL/6 mice. Cell numbers at indicated time points are shown (n = 3 mice per group per time point; left). Viral titers in the lungs were measured at the indicated time points (n = 4 mice per group per time point; middle; data are representative of at least two independent experiments; Student's t tests; P values of D are 0.0372 and 0.0043). Sections of paraffin-embedded lungs from infected mice at 6 d after infection were stained with hematoxylin/eosin (n = 3 mice per group per time point; right; data are representative of at least two independent experiments). Scale bar, 100 mm. *, P < 0.05; **, P < 0.005. All results are expressed as mean ± SEM. Arrowheads, hemorrhage; asterisks, edema; Ag, antigen; D, day; FFU, focus-forming unit; p.i., post-infection.

VPR-vaccinated groups were below the limit of detection at the time of challenge, which had no difference in half-maximum neutralizing titer in focus reduction neutralization test ($FRNT_{50}$) at 14 d.p.i. (Fig. S5), suggesting that it was virus-specific T cells, not neutralizing antibodies, that mediated the protective effect. These results indicated that vaccination-induced virus-specific T cells mediated more rapid viral clearance and decreased the extent of lung pathological changes in SARS-CoV-2–infected mice.

Cross-reactive T cell responses were found between SARS-CoV-2 and SARS-CoV infection in mice

SARS-CoV-2, SARS-CoV, and MERS-CoV are the three highly pathogenic human respiratory coronaviruses that belong to the genus *Betacoronavirus* (Petrosillo et al., 2020). The SARS-CoV-2 genome shares 79.6% and ∼40% homology with SARS-CoV and MERS-CoV, respectively, indicating that cross-reactive T cell epitopes potentially exist (Zhang et al., 2020; Zhou et al., 2020). However, identical as well as cross-reactive T cell epitopes have not been described. Previously, we had identified all the T cell epitopes in all four structural proteins in SARS-CoV–infected mice and several T cell epitopes in MERS-CoV–infected BALB/c mice (Zhao et al., 2007; Zhao et al., 2014; Zhao et al., 2010). Therefore, T cell epitopes of SARS-CoV-2 identified in infected mice in this study were compared with epitopes identified in SARS-CoV– and MERS-CoV–infected in BALB/c and C57BL/6 mice. Identical epitopes and possible cross-reactive T cell epitopes are summarized in Fig. 6 A. The core sequences of dominant CD4⁺ T cell epitopes of SARS-CoV (N353-370) and SARS-CoV-2

A

Virus	Name	Sequence
	BALB/c, MHC-II restricted	
SARS-CoV-2	N351-365	ILLNKHIDAYKTFPP
SARS-CoV	N353-370	LLNKHIDAYKTFPPTEPK
MERS-CoV	N350-362	LLEQNIDAYKTFP
	BALB/c, MHC-I restricted	
SARS-CoV-2	S535-543	KNKCVNFNF
SARS-CoV	S521-529	KNQCVNFNF
	C57BL/6, MHC-I restricted	
SARS-CoV-2	M174-181	RTLSYYKL
SARS-CoV	M173-180	RTLSYYKL
SARS-CoV-2	S510-517	VVVLSFEL
SARS-CoV	S497-504	VVLSFELL
SARS-CoV-2	S538-546	CVNFNFNGL
SARS-CoV	S525-532	VNFNFNGL

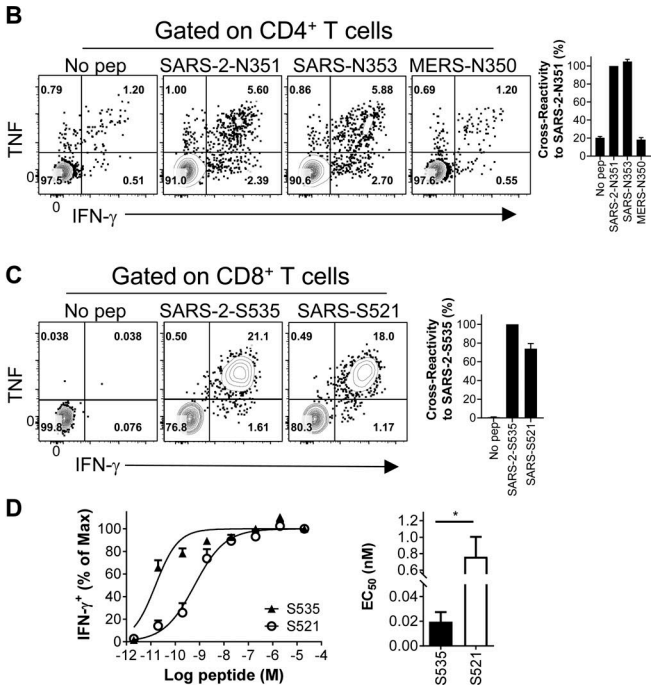

Figure 6. **Cross-reactive T cell responses were found between SARS-CoV-2 and SARS-CoV in SARS-CoV-2–infected mice. (A)** Characteristics of conserved T cell epitopes in SARS-CoV-2, SARS-CoV, and MERS-CoV. **(B and C)** BALB/c mice were transduced and infected with SARS-CoV-2. Lymphocytes derived from airway were prepared at 8 d.p.i. and stimulated with conversed epitopes. $CD4^+$ (B) and $CD8^+$ T cell responses (C) were detected by IFN-γ expression. Flow plots (left) and cross-reactivity rate (right) are shown (n = 3 or 4 mice per group; data are representative of two independent experiments). **(D)** Functional avidity curves (left) of S535-specific $CD8^+$ T cells and S521–cross-reactive $CD8^+$ T cells and the amount of peptide required for half-maximum response (EC_{50}) are shown (right; n = 3 mice; data are representative of two independent experiments; Student's t tests; P value of D is 0.0182). *, $P < 0.05$. All results are expressed as mean ± SEM. Max, maximum; pep, peptide.

(N351-365) were identical in BALB/c mice, while three amino acid differences from those of MERS-CoV (N350-362) were noted. There was one amino acid difference within the dominant $CD8^+$ T cell epitopes between SARS-CoV (S521-529) and SARS-CoV-2 (S535-543; Fig. 6 A). In C57BL/6 mice, three $CD8^+$ T cell epitopes of SARS-CoV-2 were identical to SARS-CoV. No conserved T cell epitopes between SARS-CoV-2 and MERS-CoV were found in C57BL/6 mice (Fig. 6 A).

Next, whether these potential cross-reactive T cell epitopes indeed induced cross-reactive T cell responses was examined in SARS-CoV-2–infected mice. $CD4^+$ T cells from BALF of SARS-CoV-2–infected mice responded to SARS-CoV-2 (N351-365) and SARS-CoV (N353-370) peptide stimulation, but not MERS-CoV (N350-362) peptide (Fig. 6 B). SARS-CoV (S521-529) peptide successfully stimulated $CD8^+$ T cells from SARS-CoV-2–infected BALB/c mice with >70% cross-reactivity (Fig. 6 C). As expected, cross-reactive SARS-CoV-2 (S535-543) $CD8^+$ T cells exhibited higher function avidity when stimulated with S535-543 peptide than with SARS-CoV (S521-529) peptide (Fig. 6 D). These data clearly demonstrated the existence of cross-reactive T cell responses between SARS-CoV and SARS-CoV-2 infections in BALB/c mice. Whether there is a similar cross-reactive T cell response in SARS and COVID-19 patients needs to be further studied.

Discussion

The COVID-19 pandemic represents a major public health threat and has caused a substantial increase in patient hospitalizations for pneumonia and multiorgan dysfunction. The immunopathogenesis remains unclear, which hinders the development of novel prophylactic and therapeutic measures, including vaccine design and validation.

T cells are required for many respiratory virus clearances, including SARS-CoV and MERS-CoV (Zhao et al., 2014; Zhao et al., 2011; Zhao et al., 2010). The CoV-specific T cells play indirect or direct roles in virus clearance and immune protection. In SARS-CoV–infected mice, airway memory $CD4^+$ T cells promoted respiratory dendritic cell migration by up-regulating CCR7 expression and activated STAT I pathway by producing IFN-γ, resulting in more robust cytotoxic $CD8^+$ T cell response and increased chemokine CXCL9-11 expression in the infected site tracking more virus-specific $CD8^+$ T cells (Zhao et al., 2016). However, the T cell epitopes, which are key to understanding immunopathogenesis and validating vaccines and therapeutics, remain unknown in SARS-CoV-2–infected mice. Here we identified T cell epitopes in SARS-CoV-2–infected mice using a peptide library covering all four structural proteins and six accessory proteins, including 6 I-A^d–restricted, 3 H2-K/D^d–restricted, 5 I-A^b–restricted, and 10 H2-K/D^b–restricted T cell epitopes in BALB/c and C57BL/6 mice. Dominant $CD4^+$ T cell epitopes are localized in N protein in BALB/c mice (N351) and ORF3a in C57BL/6 mice (ORF3a 266). Dominant $CD8^+$ T cell epitopes are localized in S protein in both BALB/c mice (S535) and C57BL/6 mice (S538). The selection of epitopes for T cell recognition is MHC-restricted, so epitopes that are recognized

by T cells from BALB/c and C57BL/6 mice are different. $CD8^+$ T cell responses in C57BL/6 mice were more robust than those of BALB/c mice, which may contribute to more rapid viral clearance in C57BL/6 mice (Sun et al., 2020).

Airway virus–specific T cells provide the first line of defense against challenge, enhancing the immune response early after infection. Airway-derived SARS-CoV-2–specific $CD4^+$ T cells and $CD8^+$ T cells are superior effector cells compared with those from lung parenchyma, consistent with previous studies (Zhao et al., 2016). In IFNAR KO mice, frequency and numbers of total and of polyfunctional virus-specific T cells, as well as sensitivity upon antigen stimulation, were reduced, resulting in delayed viral clearance, indicating that IFN-I signaling is required for optimal SARS-CoV-2–specific T cell generation and function. Consistent with this, immunocompromised COVID-19 patients had higher viral loads, rates of hospitalization, intensive care unit admissions, and severe respiratory illness (Robilotti et al., 2020).

To address whether virus-specific memory T cells alone could mediate long-term protection, VRP vectors expressing single SARS-CoV-2–specific $CD4^+$ or $CD8^+$ T cell epitopes were generated. Mice could be partially protected from SARS-CoV-2 infection 4 wk after VRP vaccination as determined by moderate reduced viral titers and diminished lesions in the lungs. This experiment provided direct evidence showing the protective role of memory T cells.

Last, several cross-reactive T cell epitopes in both BALB/c and C57BL/6 mice between SARS-CoV and SARS-CoV-2 but not MERS-CoV were identified in this study. No licensed vaccines are available for either SARS-CoV-2 or SARS-CoV. A long-lasting vaccine that induces broad protection against several CoVs would be useful and might provide long-term protection against additional SARS-like CoV that might arise in the future.

In summary, we demonstrate that SARS-CoV-2 induced robust T cell responses in mice. T cell epitopes were identified in both BALB/c and C57BL/6 mice in this study. SARS-CoV-2–specific $CD4^+$ T and $CD8^+$ T cells were polyfunctional, and were able to lyse target cells in vivo, which protected mice from SARS-CoV-2 infection in the absence of neutralizing antibodies. Further, IFN-I pathway was proved to be critical to generating optimal antiviral T cell responses after SARS-CoV-2 infection. In addition, cross-reactive T cell responses were found between SARS-CoV and SARS-CoV-2 in mice, but not MERS-CoV. The identification of T cell epitopes and characterization of T cell responses will not only aid immunopathogenesis studies of COVID-19 disease in mice but also help vaccine design and validation in vivo.

Materials and methods

Mice, virus, and cells

Specific pathogen–free 6–8-wk-old BALB/c and C57BL/6 mice were purchased from Hunan SJA Laboratory Animal Co. $IFNAR^{-/-}$ mice on BALB/c background were gifts from Dr. Stanley Perlman (University of Iowa, Iowa City, IA) and were backcrossed to BALB/c background for 10 generations. All protocols were approved by the Institutional Animal Care and Use Committees of Guangzhou Medical University. The SARS-CoV-2 strains used in this study were isolated from COVID-19 patients in Guangzhou (GenBank accession no. MT123290) and passaged on Vero E6 cells. African Green monkey kidney–derived Vero E6 cells were grown in DMEM (GIBCO) supplemented with 10% FBS (GIBCO). Mouse-derived A20 and CHB3 cells were grown in RPMI 1640 medium (GIBCO) supplemented with 10% FBS.

Chemicals, cytokines, and peptides

A set of 20-mer peptides encompassing the four SARS-CoV-2 structural (S glycoprotein, N protein, and M and E proteins) and six putative accessory proteins (ORF3a [25396–26223], ORF6 [27205–27390], ORF7a [27397–27762], ORF8 [27897–28262], ORF9b [28287–28580], and ORF9c [28737–28958]) overlapping by 10 amino acids, and all truncated 8–9-mer or 13–15-mer peptides were synthesized by GL Biochem Ltd. and used for stimulation of T cells.

Transduction and infection of mice

Mice were lightly anesthetized with isoflurane (RWD Life Science) and transduced i.n. with 2.5×10^8 focus-forming units of Ad5-ACE2 in 75 µl DMEM. 5 d after transduction, mice were infected i.n. with SARS-CoV-2 (1×10^5 PFU) in a total volume of 50 µl DMEM. Mice were examined at indicated time points after infection. All work with SARS-CoV-2 was conducted in the Biosafety Level 3 Laboratories of Guangzhou Customs District Technology Center (Sun et al., 2020).

Focus-forming assay

Vero E6 cells were seeded in 96-well plates 1 d before infection. Lung homogenates were serially diluted and used to inoculate Vero E6 cells at 37°C for 1 h. Inocula were then removed before adding 125 µl 37°C prewarmed 1.6% carboxymethylcellulose (Sigma-Aldrich) per well. After 24 h, cells were fixed with 4% paraformaldehyde (Biosharp Life Sciences) and permeabilized with 0.2% Triton X-100 (Solarbio). Cells were then incubated with a rabbit anti–SARS-CoV N protein polyclonal antibody (40143-T62; Sino Biological, Inc.) followed by an HRP-labeled goat anti-rabbit secondary antibody (109-035-088; Jackson ImmunoResearch Laboratories, Inc.). The foci were visualized by TrueBlue Peroxidase Substrate (KPL) and counted with an ELISPOT reader (Cellular Technology Ltd.). Viral titers were calculated as focus-forming units per milliliter or per gram tissue.

FRNT

To detect neutralizing antibodies in mouse plasma, SARS-CoV-2 FRNT was performed in a certified biosafety level 3 laboratory. 50 µl plasma samples were serially diluted, mixed with 50 µl of SARS-CoV-2 incubated for 1 h at 37°C. Mixtures were then transferred to 96-well plates seeded with Vero E6 cells (ATCC) and incubated for 1 h at 37°C to allow virus entry. The next steps were the same as the focus-forming assay. $FRNT_{50}$ was half-maximum neutralizing titer (Wang et al., 2020).

VRPs and mouse immunization

VRPs expressing the four SARS-CoV-2 structural (S glycoprotein, N protein, and M and E proteins), six accessory proteins

(ORF3a, ORF6, ORF7a, ORF8, ORF9b, and ORF9c), and indicated T cell epitopes were constructed as previously described (Zhao et al., 2014). Mice were vaccinated once or twice at 4-wk intervals with 10^5 infectious units of VRP i.n. in 50 µl of Dulbecco's PBS after light anesthesia with isoflurane. BALF or lung was harvested at 7 d after prime or 5 d after boost. For SARS-CoV-2 infection after vaccination, mice were challenged 4 wk after VRP boost.

Preparation of cells from BALF, lungs, DLNs, and spleens

Mice were sacrificed at the indicated time points. BALF was acquired by inflating lungs with 1 ml complete RPMI 1640 medium via cannulation of the trachea followed by lavaging four times. Cells in the BALF were collected by centrifugation. Cells were prepared from the lungs, DLN, and spleen as previously described (Zhao et al., 2011). The lung vascular bed was flushed via the right ventricle with 10 ml Dulbecco's PBS (GIBCO), and lungs, DLNs, and spleens were then removed. Lungs were cut into small pieces and digested in HBSS buffer (GIBCO) containing 2% FCS, 25 mM Hepes (GIBCO), 1 mg/ml collagenase D (Roche), and 0.1 mg/ml DNase (Roche) for 30 min at room temperature. DLNs and spleens were minced and pressed though a wire screen. Particulate matter was removed with a 70-µm filter (Corning) to obtain single-cell suspensions.

Flow cytometry

The following monoclonal antibodies were used: rat anti-mouse CD8α-Alexa 488 (clone 53–6.7; 100723; Biolegend), anti-mouse CD16/32-PerCP-Cy5.5 (clone 93; 45–0161-82; eBioscience), anti-mouse CD4-eFluor 450 (clone RM4-5; 48–0042-82; eBioscience), anti-mouse CD4-Brilliant Violet 510 (clone GK1.5; 100449; Biolegend), anti-mouse TNF-PE (clone MP6-XT22; 12–7321-82; eBioscience), anti-mouse TNF-PE-Cyanine7 (clone MP6-XT22; 25–7321-82; eBioscience), anti-mouse IFN-γ-APC (cloneXMG1.2; 17–7311-82; eBioscience), anti-mouse IFN-γ-eFluor 450 (clone XMG1.2; 48–7311-82; eBioscience), anti-mouse IL-2-PE (clone JES6-5H4; 503808; Biolegend), and anti-mouse IL-10-APC (clone JES5-16E3; 505010; Biolegend), anti-mouse I-A/I-E-PerCP/Cyanine5.5 (clone M5/114.15.2; 107625; Biolegend), anti-mouse CD45.1-APC (clone A20; 110713; Biolegend), anti-mouse CD107a (LAMP-1)-A488 (clone 1D4B; 121607; Biolegend), granzyme B monoclonal antibody (NGZB)-PE (clone NGZB; 12–8898-82; eBioscience), anti-mouse CD195 (CCR5)-PE (clone HM-CCR5; 107005; Biolegend), anti-mouse CD183 (CXCR3)-APC (clone CXCR3-173; 126512; Biolegend), anti-mouse CD186 (CXCR6)-PE (clone SA051D1; 151103; Biolegend), anti-mouse CD62L-FITC (clone MEL-14; 104406; Biolegend), anti-mouse/human CD44-PE (clone IM7; 103007; Biolegend), anti-mouse CD197 (CCR7)-APC (clone 4B12; 17–1971-82; eBioscience), anti-mouse Ly-6C-PE (clone AL-21; 560592; eBioscience), anti-mouse CD103-A488 (clone 2E7; 121407; Biolegend), anti-mouse CD43-PE (clone 1B11; 121207; Biolegend), anti-mouse CD69-APC (clone H1.2F3; 104513; Biolegend), anti-mouse CD11a-A488 (clone M17/4; 101111; Biolegend), anti-mouse CD49d-APC (clone R1-2; 103621; Biolegend), anti-mouse CD154-APC (clone MR1; 106509; Biolegend), anti-mouse CD127 (IL-7Rα)-PE (clone A7R34; 135009; Biolegend), anti-mouse CD279 (PD-1)-PE (clone RMP1-30; 109103; Biolegend), rat IgG1, κ isotype control antibody-PE (clone RTK2071; 400408; Biolegend), rat IgM, κ isotype control antibody-FITC (clone RTK2118; 400805; Biolegend), Armenian hamster IgG isotype control antibody-APC (clone HTK888; 400911; Biolegend), Armenian hamster IgG isotype control antibody-PE (clone HTK888; 400907; Biolegend), rat IgG2b, κ isotype control antibody-PE (clone RTK4530; 400608; Biolegend), rat IgG2b, κ isotype control antibody-APC (clone RTK4530; 400612; Biolegend), rat IgG2a, κ isotype control antibody-FITC (clone RTK2758; 400505; Biolegend), rat IgG2a, κ isotype control antibody-A488 (clone RTK2758; 400525; Biolegend), and rat IgG2a, κ isotype control antibody-APC (clone RTK2758; 400512; Biolegend). For ICS, lymphocytes were cultured in 96-well plates at 37°C for 5–6 h in the presence of indicated peptides and brefeldin A (BD Biosciences). Cells were then labeled for cell surface markers at 4°C for 15 min in the dark, fixed/permeabilized with Cytofix/Cytoperm Solution (BD Biosciences), and labeled with intracellular antibody cocktails. All flow cytometry data were acquired on a BD FACSVerse Cytometer and were analyzed using FlowJo software.

Histology

Animals were anesthetized and transcardially perfused with PBS followed by zinc formalin (Sigma-Aldrich). Lungs were fixed in zinc formalin. For routine histology, tissue sections (~4 µm each) were stained with hematoxylin and eosin.

In vivo cytotoxicity assay

In vivo cytotoxicity assays were performed 8 d.p.i. Briefly, splenocytes from CD45.1 congenic naive mice were stained with either 2 µM or 100 nM CFSE (Molecular Probes) and then pulsed with the indicated peptides (10 µM for $CD4^+$ T epitope and 2 µM for $CD8^+$ T epitope) or vehicle at 37°C for 1 h. Then, 5×10^5 cells from each group were mixed together (10^6 cells in total) and transferred i.n. into mice. At 16 h after transfer, total lung cells were isolated. Target cells were identified on the basis of CD45.1 staining and were distinguished from each other by differential CFSE staining. After gating on $CD45.1^+$ cells, the percentage lysis was calculated as previously described (Zhao et al., 2009), using the following equation: killing (%) = 100 − 100 × (% peptide pulsed in infected / % peptide unpulsed in infected) / (% peptide pulsed in mock / % peptide unpulsed in mock).

Statistical analysis

Student's *t* tests were used to analyze differences in mean values between groups using GraphPad Prism 7. All results are expressed as mean ± SEM and were corrected for multiple comparisons. P values of <0.05 were considered statistically significant (*, $P < 0.05$; **, $P < 0.005$; ***, $P < 0.0005$; ****, $P < 0.0001$).

Online supplemental material

Fig. S1 shows the results of mapping SARS-CoV-2 T cell epitopes in VRP-vaccinated BALB/c mice. Fig. S2 shows the results of mapping SARS-CoV-2 T cell epitopes in VRP-vaccinated C57BL/6 mice. Fig. S3 shows the kinetics of virus-specific T cell responses in DLNs and spleens of SARS-CoV-2–infected BALB/c and

C57BL/6 mice. Fig. S4 shows SARS-CoV-2–specific CD8⁺ T cells were polyfunctional in infected C57BL/6 mice. Fig. S5 shows there are no neutralizing antibodies in BALB/c mice at the time of challenge.

Acknowledgments

We thank Prof. Stanley Perlman (University of Iowa) for critical reading of the manuscript and helpful comments.

This work is supported by grants from the National Key Research and Development Program of China (2018YFC1200100, 2020YFC0842400), National Natural Science Foundation of China (82025001, 91842106, 81901623), Ministries of Science and Technology of Guangdong Province (2020B1111330001, 2020A111128008, 2020B1111320003, B195001248), Ministries of Education of Guangdong Province (2020KZDZX1158), Science and Technology Planning Project of Guangzhou (202008040005), Science and Technology Planning Project of Guangdong Province (2018A030310177), and the State Key Laboratory of Respiratory Disease Science and Technology Foundation (SKLRD-QN-201912).

Author contributions: Jincun Zhao, Z. Zhuang, Jingxian Zhao, and D. Zhou designed and coordinated the study. Z. Zhuang, X. Lai, J. Sun, Z. Chen, Z. Zhang, J. Dai, D. Liu, Y. Li, and F. Li performed the experiments. Z. Zhuang, Jincun Zhao, and Jingxian Zhao wrote the manuscript. Jincun Zhao, Z. Zhuang, Jingxian Zhao, and D. Zhou reviewed and edited the manuscript. Jincun Zhao, D. Zhou, Jingxian Zhao, Z. Zhuang, X. Lai, J. Sun, Z. Chen, Z. Zhang, J. Dai, D. Liu, Y. Li, F. Li, Y. Wang, A. Zhu, J. Wang, W. Yang, J. Huang, X. Li, L. Hu, L. Wen, J. Zhuo, Y. Zhang, D. Chen, S. Li, S. Huang, Y. Shi, K. Zheng, and N. Zhong contributed to the interpretation and conclusions presented.

Disclosures: The authors declare no competing interests exist.

Submitted: 12 October 2020
Revised: 6 December 2020
Accepted: 22 December 2020

References

Braun, J., L. Loyal, M. Frentsch, D. Wendisch, P. Georg, F. Kurth, S. Hippenstiel, M. Dingeldey, B. Kruse, F. Fauchere, et al. 2020. SARS-CoV-2-reactive T cells in healthy donors and patients with COVID-19. *Nature.* 587:270–274. https://doi.org/10.1038/s41586-020-2598-9

Brien, J.D., J.L. Uhrlaub, and J. Nikolich-Zugich. 2008. West Nile virus-specific CD4 T cells exhibit direct antiviral cytokine secretion and cytotoxicity and are sufficient for antiviral protection. *J. Immunol.* 181: 8568–8575. https://doi.org/10.4049/jimmunol.181.12.8568

Brummelman, J., K. Pilipow, and E. Lugli. 2018. The Single-Cell Phenotypic Identity of Human CD8⁺ and CD4⁺ T Cells. *Int. Rev. Cell Mol. Biol.* 341: 63–124. https://doi.org/10.1016/bs.ircmb.2018.05.007

Christensen, J.P., P.C. Doherty, K.C. Branum, and J.M. Riberdy. 2000. Profound protection against respiratory challenge with a lethal H7N7 influenza A virus by increasing the magnitude of CD8(+) T-cell memory. *J. Virol.* 74: 11690–11696. https://doi.org/10.1128/JVI.74.24.11690-11696.2000

Coler, R.N., T. Hudson, S. Hughes, P.W. Huang, E.A. Beebe, and M.T. Orr. 2015. Vaccination Produces CD4 T Cells with a Novel CD154-CD40-Dependent Cytolytic Mechanism. *J. Immunol.* 195:3190–3197. https://doi.org/10.4049/jimmunol.1501118

Dhanda, S.K., S. Mahajan, S. Paul, Z. Yan, H. Kim, M.C. Jespersen, V. Jurtz, M. Andreatta, J.A. Greenbaum, P. Marcatili, et al. 2019. IEDB-AR: immune epitope database-analysis resource in 2019. *Nucleic Acids Res.* 47(W1): W502–W506. https://doi.org/10.1093/nar/gkz452

Di Cosimo, S., L. Porcu, A. Malfettone, J. Cortés, and R. Miceli. 2020. Commentary: SARS-CoV-2 Transmission in Patients With Cancer at a Tertiary Care Hospital in Wuhan, China. *Front. Oncol.* 10:1223. https://doi.org/10.3389/fonc.2020.01223

González-Navajas, J.M., J. Lee, M. David, and E. Raz. 2012. Immunomodulatory functions of type I interferons. *Nat. Rev. Immunol.* 12:125–135. https://doi.org/10.1038/nri3133

Grifoni, A., D. Weiskopf, S.I. Ramirez, J. Mateus, J.M. Dan, C.R. Moderbacher, S.A. Rawlings, A. Sutherland, L. Premkumar, R.S. Jadi, et al. 2020. Targets of T Cell Responses to SARS-CoV-2 Coronavirus in Humans with COVID-19 Disease and Unexposed Individuals. *Cell.* 181: 1489–1501.e15. https://doi.org/10.1016/j.cell.2020.05.015

Kim, D., J.Y. Lee, J.S. Yang, J.W. Kim, V.N. Kim, and H. Chang. 2020. The Architecture of SARS-CoV-2 Transcriptome. *Cell.* 181:914–921.e10. https://doi.org/10.1016/j.cell.2020.04.011

Le Bert, N., A.T. Tan, K. Kunasegaran, C.Y.L. Tham, M. Hafezi, A. Chia, M.H.Y. Chng, M. Lin, N. Tan, M. Linster, et al. 2020. SARS-CoV-2-specific T cell immunity in cases of COVID-19 and SARS, and uninfected controls. *Nature.* 584:457–462. https://doi.org/10.1038/s41586-020-2550-z

Mateus, J., A. Grifoni, A. Tarke, J. Sidney, S.I. Ramirez, J.M. Dan, Z.C. Burger, S.A. Rawlings, D.M. Smith, E. Phillips, et al. 2020. Selective and cross-reactive SARS-CoV-2 T cell epitopes in unexposed humans. *Science.* 370: 89–94. https://doi.org/10.1126/science.abd3871

McDermott, D.S., and S.M. Varga. 2011. Quantifying antigen-specific CD4 T cells during a viral infection: CD4 T cell responses are larger than we think. *J. Immunol.* 187:5568–5576. https://doi.org/10.4049/jimmunol.1102104

McNab, F., K. Mayer-Barber, A. Sher, A. Wack, and A. O'Garra. 2015. Type I interferons in infectious disease. *Nat. Rev. Immunol.* 15:87–103. https://doi.org/10.1038/nri3787

Peng, Y., A.J. Mentzer, G. Liu, X. Yao, Z. Yin, D. Dong, W. Dejnirattisai, T. Rostron, P. Supasa, C. Liu, et al. 2020. Broad and strong memory CD4 (+) and CD8 (+) T cells induced by SARS-CoV-2 in UK convalescent COVID-19 patients. *bioRxiv* https://doi.org/ (Preprint posted June 8, 2020). https://doi.org/10.1101/2020.06.05.13455

Perry, A.K., G. Chen, D. Zheng, H. Tang, and G. Cheng. 2005. The host type I interferon response to viral and bacterial infections. *Cell Res.* 15: 407–422. https://doi.org/10.1038/sj.cr.7290309

Peters, P.J., J. Borst, V. Oorschot, M. Fukuda, O. Krähenbühl, J. Tschopp, J.W. Slot, and H.J. Geuze. 1991. Cytotoxic T lymphocyte granules are secretory lysosomes, containing both perforin and granzymes. *J. Exp. Med.* 173:1099–1109. https://doi.org/10.1084/jem.173.5.1099

Petrosillo, N., G. Viceconte, O. Ergonul, G. Ippolito, and E. Petersen. 2020. COVID-19, SARS and MERS: are they closely related? *Clin. Microbiol. Infect.* 26:729–734. https://doi.org/10.1016/j.cmi.2020.03.026

Pushko, P., M. Parker, G.V. Ludwig, N.L. Davis, R.E. Johnston, and J.F. Smith. 1997. Replicon-helper systems from attenuated Venezuelan equine encephalitis virus: expression of heterologous genes in vitro and immunization against heterologous pathogens in vivo. *Virology.* 239:389–401. https://doi.org/10.1006/viro.1997.8878

Rai, D., N.L. Pham, J.T. Harty, and V.P. Badovinac. 2009. Tracking the total CD8 T cell response to infection reveals substantial discordance in magnitude and kinetics between inbred and outbred hosts. *J. Immunol.* 183:7672–7681. https://doi.org/10.4049/jimmunol.0902874

Rammensee, H.G. 1995. Chemistry of peptides associated with MHC class I and class II molecules. *Curr. Opin. Immunol.* 7:85–96. https://doi.org/10.1016/0952-7915(95)80033-6

Reche, P.A., J.P. Glutting, H. Zhang, and E.L. Reinherz. 2004. Enhancement to the RANKPEP resource for the prediction of peptide binding to MHC molecules using profiles. *Immunogenetics.* 56:405–419. https://doi.org/10.1007/s00251-004-0709-7

Robilotti, E.V., N.E. Babady, P.A. Mead, T. Rolling, R. Perez-Johnston, M. Bernardes, Y. Bogler, M. Caldararo, C.J. Figueroa, M.S. Glickman, et al. 2020. Determinants of COVID-19 disease severity in patients with cancer. *Nat. Med.* 26:1218–1223. https://doi.org/10.1038/s41591-020-0979-0

Sekine, T., A. Perez-Potti, O. Rivera-Ballesteros, K. Strålin, J.B. Gorin, A. Olsson, S. Llewellyn-Lacey, H. Kamal, G. Bogdanovic, S. Muschiol, et al. Karolinska COVID-19 Study Group. 2020. Robust T Cell Immunity in Convalescent Individuals with Asymptomatic or Mild COVID-19. *Cell.* 183:158–168.e14. https://doi.org/10.1016/j.cell.2020.08.017

Sun, J., R. Madan, C.L. Karp, and T.J. Braciale. 2009. Effector T cells control lung inflammation during acute influenza virus infection by producing IL-10. *Nat. Med.* 15:277–284. https://doi.org/10.1038/nm.1929

Sun, J., Z. Zhuang, J. Zheng, K. Li, R.L. Wong, D. Liu, J. Huang, J. He, A. Zhu, J. Zhao, et al. 2020. Generation of a Broadly Useful Model for COVID-19 Pathogenesis, Vaccination, and Treatment. *Cell*. 182:734–743.e5. https://doi.org/10.1016/j.cell.2020.06.010

Wang, Y., L. Zhang, L. Sang, F. Ye, S. Ruan, B. Zhong, T. Song, A.N. Alshukairi, R. Chen, Z. Zhang, et al. 2020. Kinetics of viral load and antibody response in relation to COVID-19 severity. *J. Clin. Invest.* 130:5235–5244. https://doi.org/10.1172/JCI138759

Weiskopf, D., K.S. Schmitz, M.P. Raadsen, A. Grifoni, N.M.A. Okba, H. Endeman, J.P.C. van den Akker, R. Molenkamp, M.P.G. Koopmans, E.C.M. van Gorp, et al. 2020. Phenotype and kinetics of SARS-CoV-2-specific T cells in COVID-19 patients with acute respiratory distress syndrome. *Sci. Immunol.* 5:eabd2071. https://doi.org/10.1126/sciimmunol.abd2071

Yamanouchi, S., K. Kuwahara, A. Sakata, T. Ezaki, S. Matsuoka, J. Miyazaki, S. Hirose, T. Tamura, H. Nariuchi, and N. Sakaguchi. 1998. A T cell activation antigen, Ly6C, induced on CD4+ Th1 cells mediates an inhibitory signal for secretion of IL-2 and proliferation in peripheral immune responses. *Eur. J. Immunol.* 28:696–707. https://doi.org/10.1002/(SICI)1521-4141(199802)28:02<696::AID-IMMU696>3.0.CO;2-N

Zhang, X.Y., H.J. Huang, D.L. Zhuang, M.I. Nasser, M.H. Yang, P. Zhu, and M.Y. Zhao. 2020. Biological, clinical and epidemiological features of COVID-19, SARS and MERS and AutoDock simulation of ACE2. *Infect. Dis. Poverty*. 9:99. https://doi.org/10.1186/s40249-020-00691-6

Zhao, J., Q. Huang, W. Wang, Y. Zhang, P. Lv, and X.M. Gao. 2007. Identification and characterization of dominant helper T-cell epitopes in the nucleocapsid protein of severe acute respiratory syndrome coronavirus. *J. Virol.* 81:6079–6088. https://doi.org/10.1128/JVI.02568-06

Zhao, J., J. Zhao, N. Van Rooijen, and S. Perlman. 2009. Evasion by stealth: inefficient immune activation underlies poor T cell response and severe disease in SARS-CoV-infected mice. *PLoS Pathog.* 5:e1000636. https://doi.org/10.1371/journal.ppat.1000636

Zhao, J., J. Zhao, and S. Perlman. 2010. T cell responses are required for protection from clinical disease and for virus clearance in severe acute respiratory syndrome coronavirus-infected mice. *J. Virol.* 84:9318–9325. https://doi.org/10.1128/JVI.01049-10

Zhao, J., J. Zhao, K. Legge, and S. Perlman. 2011. Age-related increases in PGD(2) expression impair respiratory DC migration, resulting in diminished T cell responses upon respiratory virus infection in mice. *J. Clin. Invest.* 121:4921–4930. https://doi.org/10.1172/JCI59777

Zhao, J., K. Li, C. Wohlford-Lenane, S.S. Agnihothram, C. Fett, J. Zhao, M.J. Gale Jr., R.S. Baric, L. Enjuanes, T. Gallagher, et al. 2014. Rapid generation of a mouse model for Middle East respiratory syndrome. *Proc. Natl. Acad. Sci. USA.* 111:4970–4975. https://doi.org/10.1073/pnas.1323279111

Zhao, J., J. Zhao, A.K. Mangalam, R. Channappanavar, C. Fett, D.K. Meyerholz, S. Agnihothram, R.S. Baric, C.S. David, and S. Perlman. 2016. Airway Memory CD4(+) T Cells Mediate Protective Immunity against Emerging Respiratory Coronaviruses. *Immunity*. 44:1379–1391. https://doi.org/10.1016/j.immuni.2016.05.006

Zhao, J., A.N. Alshukairi, S.A. Baharoon, W.A. Ahmed, A.A. Bokhari, A.M. Nehdi, L.A. Layqah, M.G. Alghamdi, M.M. Al Gethamy, A.M. Dada, et al. 2017. Recovery from the Middle East respiratory syndrome is associated with antibody and T-cell responses. *Sci. Immunol.* 2:eaan5393. https://doi.org/10.1126/sciimmunol.aan5393

Zhong, W., A.D. Roberts, and D.L. Woodland. 2001. Antibody-independent antiviral function of memory CD4+ T cells in vivo requires regulatory signals from CD8+ effector T cells. *J. Immunol.* 167:1379–1386. https://doi.org/10.4049/jimmunol.167.3.1379

Zhou, Y., J. Zha, Z. Lin, Z. Fang, H. Zeng, J. Zhao, Y. Luo, Z. Li, and B. Xu. 2018. CD4+ T cell-mediated cytotoxicity is associated with MHC class II expression on malignant CD19+ B cells in diffuse large B cell lymphoma. *Exp. Cell Res.* 362:287–292. https://doi.org/10.1016/j.yexcr.2017.11.029

Zhou, P., X.L. Yang, X.G. Wang, B. Hu, L. Zhang, W. Zhang, H.R. Si, Y. Zhu, B. Li, C.L. Huang, et al. 2020. A pneumonia outbreak associated with a new coronavirus of probable bat origin. *Nature*. 579:270–273. https://doi.org/10.1038/s41586-020-2012-7

Supplemental material

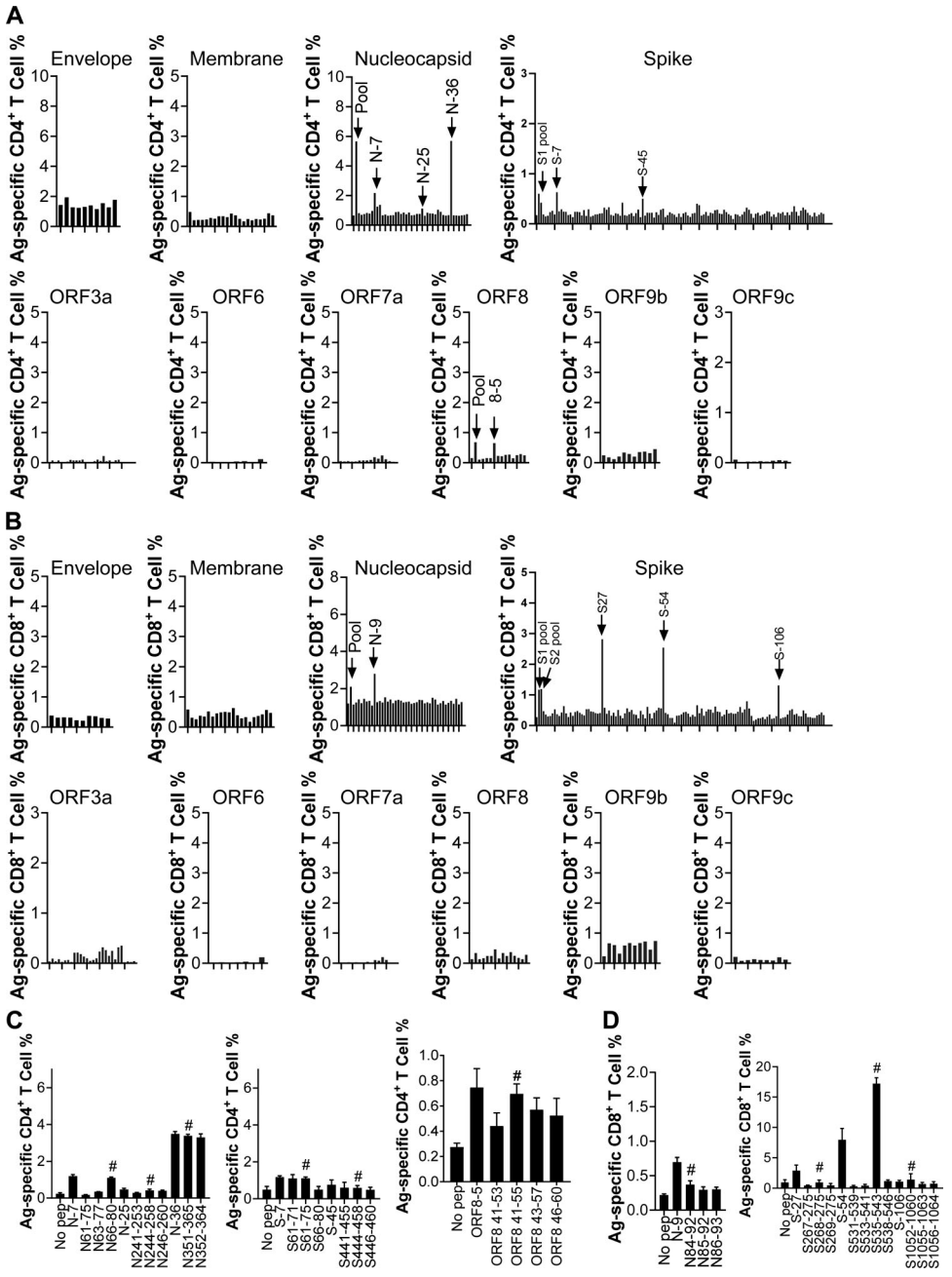

Figure S1. **Mapping SARS-CoV-2 T cell epitopes in BALB/c mice. (A)** Lymphocytes from vaccinated lungs were stimulated with 5 µM 20-mer (20 amino acids) peptides. Antigen-specific CD4⁺ T cell responses were determined by intracellular IFN-γ staining. **(B)** Lymphocytes from vaccinated lungs were stimulated with 5 µM 20-mer (20 amino acids) peptides. Antigen-specific CD8⁺ T cell responses were determined. **(C)** Lymphocytes from vaccinated lungs were stimulated with 5 µM 20-mer (20 amino acids) and corresponding truncated 13–15-mer peptides for 5–6 h in the presence of brefeldin A. Antigen-specific CD4⁺ T cell responses were determined. **(D)** Lymphocytes from vaccinated lungs were stimulated with 5 µM 20-mer (20 amino acids) and corresponding truncated 8–9-mer peptides for 5–6 h in the presence of brefeldin A. Antigen-specific CD8⁺ T cell responses were determined. Candidate truncated epitopes are labeled with # (n = 3; data are representative of at least two independent experiments). All results are expressed as mean ± SEM. Ag, antigen; pep, peptide.

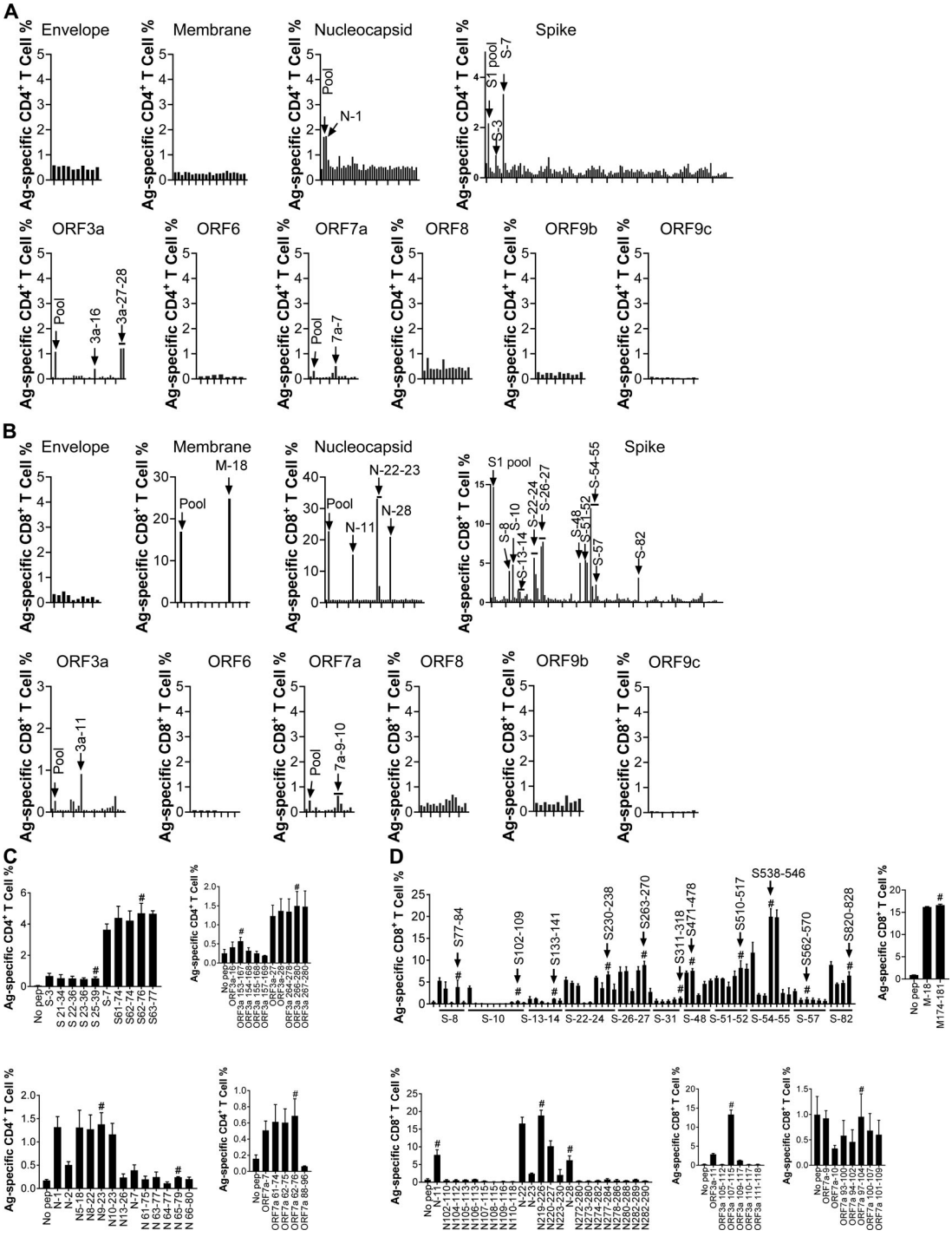

Figure S2. **Mapping SARS-CoV-2 T cell epitopes in C57BL/6 mice. (A)** Lymphocytes from vaccinated lungs were stimulated with 5 µM 20-mer (20 amino acids) peptides. Antigen-specific CD4⁺ T cell responses were determined by intracellular IFN-γ staining. **(B)** Lymphocytes from vaccinated lungs were stimulated with 5 µM 20-mer (20 amino acids) peptides. Antigen-specific CD8⁺ T cell responses were determined. **(C)** Lymphocytes from vaccinated lungs were stimulated with 5 µM 20-mer (20 amino acids) and corresponding truncated 13–15-mer peptides. Antigen-specific CD4⁺ T cell responses were determined. **(D)** Lymphocytes from vaccinated lungs were stimulated with 5 µM 20-mer (20 amino acids) and corresponding truncated 8–9-mer peptides. Antigen-specific CD8⁺ T cell responses were determined. Candidate truncated epitopes are labeled with # (n = 3; data are representative of at least two independent experiments). All results are expressed as mean ± SEM. Ag, antigen; pep, peptide.

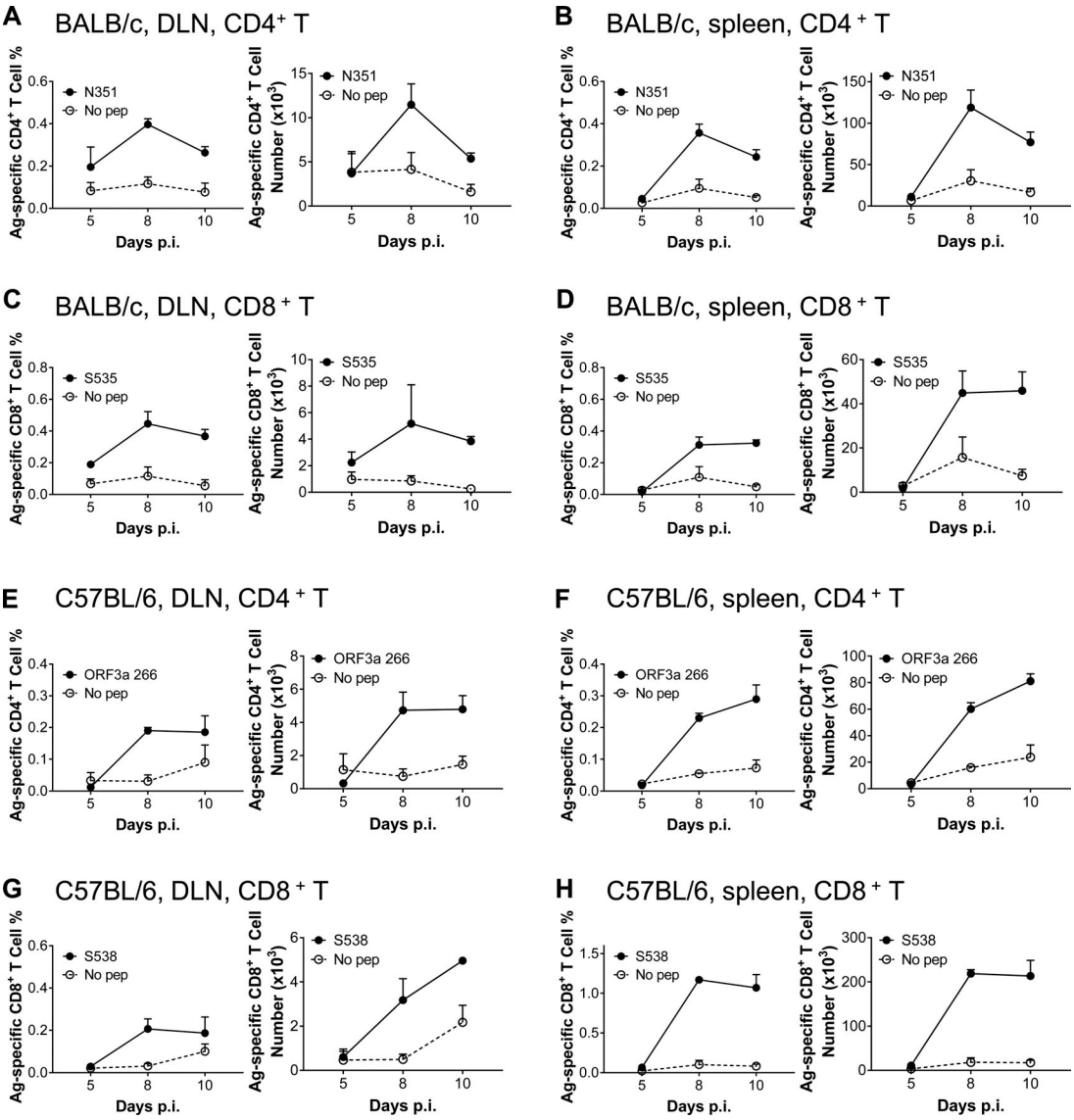

Figure S3. **Kinetics of virus-specific T cell responses in DLNs and spleens of SARS-CoV-2–infected BALB/c and C57BL/6 mice. (A–D)** Lymphocytes from DLN and spleen of transduced/infected WT BALB/c mice were harvested at indicated time points after infection and stimulated with 5 µM N351 (A and B) and 1 µM S535 (C and D) for 6 h in the presence of brefeldin A. The frequencies (left) and cell numbers of antigen-specific T cells (right) in DLN (A and C) and spleen (B and D) are shown (n = 3 mice; data are representative of one experiment). **(E–H)** Lymphocytes from DLN and spleen of transduced/infected C57BL/6 mice were harvested at indicated time points and stimulated with 5 µM ORF3a 266 (E and F) and 1 µM S538 (G and H) for 6 h in the presence of brefeldin A. The frequencies (left) and cell numbers (right) of antigen-specific T cells are shown (n = 3; data are representative of one experiment). All results are expressed as mean ± SEM. Ag, antigen; pep, peptide; p.i., post-infection.

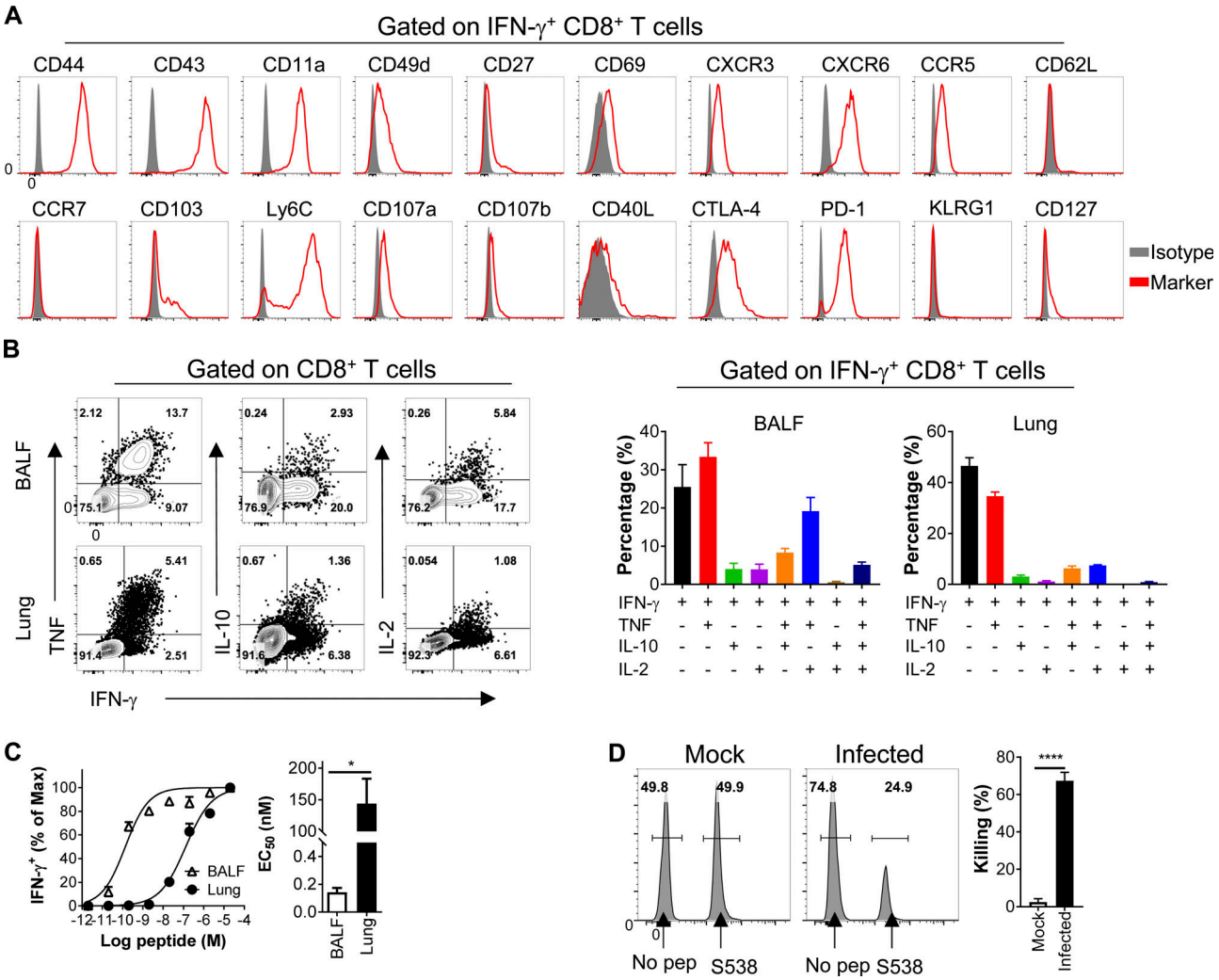

Figure S4. **SARS-CoV-2–specific CD8⁺ T cells were polyfunctional in infected C57BL/6 mice. (A)** Cells from BALF were stained with antibodies against the indicated markers. Histograms shown here were gated on SARS-CoV-2-S538–specific CD8⁺ T cells. **(B)** Cytokine expression of airway derived SARS-CoV-2-S538–specific CD8⁺ T cells are shown (n = 3 or 4 mice; data are representative of one experiment). **(C)** Functional avidity curves (left) of airway- and lung-derived SARS-CoV-2-S538–specific CD8⁺ T cells and the amount of peptide required for half-maximum response (EC_{50}) are shown (right; n = 3; data are representative of two independent experiments; Student's t tests; P value of C is 0.011). **(D)** Representative flow histograms (left) and killing rates (right) of in vivo cytotoxicity of SARS-CoV-2-S538–specific CD8⁺ T cells in SARS-CoV-2–infected mice and mock-infected mice are shown (n = 5; data are representative of one experiment; Student's t tests; P value of C is <0.0001). ****, P < 0.0001. All results are expressed as mean ± SEM. Max, maximum; pep, peptide.

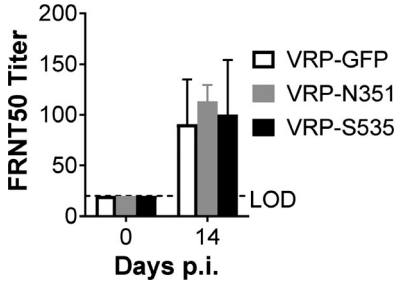

Figure S5. **No neutralizing antibodies in BALB/c mice at the time of challenge.** Neutralizing antibodies titers in the sera of vaccinated and infected BALB/c mice at time of challenge and 14 d.p.i. (n = 6; data are representative of one experiment). All results are expressed as mean ± SEM. LOD, limit of detection; p.i., post-infection.